

Eikonal quasinormal modes of black holes beyond general relativity. III. Scalar Gauss-Bonnet gravity

Albert Bryant,¹ Hector O. Silva,^{2,3} Kent Yagi¹ , and Kostas Glampedakis^{4,5}

¹*Department of Physics, University of Virginia, Charlottesville, Virginia 22904-4714, USA*

²*Max Planck Institute for Gravitational Physics (Albert Einstein Institute),
Am Mühlenberg 1, Potsdam 14476, Germany*

³*Illinois Center for Advanced Studies of the Universe & Department of Physics,
University of Illinois at Urbana-Champaign, Urbana, Illinois 61801, USA*

⁴*Departamento de Física, Universidad de Murcia, Murcia E-30100, Spain*

⁵*Theoretical Astrophysics, University of Tübingen, Auf der Morgenstelle 10, Tübingen D-72076, Germany*



(Received 17 June 2021; accepted 12 July 2021; published 20 August 2021)

In a recent series of papers, we have shown how the eikonal/geometrical optics approximation can be used to calculate analytically the fundamental quasinormal mode frequencies associated with coupled systems of wave equations, which arise, for instance, in the study of perturbations of black holes in gravity theories beyond General Relativity. As a continuation to this series, we focus here on the quasinormal modes of nonrotating black holes in scalar Gauss-Bonnet gravity assuming a small-coupling expansion. We show that the axial perturbations are purely tensorial and are described by a modified Regge-Wheeler equation, while the polar perturbations are of mixed scalar-tensor character and are described by a system of two coupled wave equations. When applied to these equations, the eikonal machinery leads to axial quasinormal modes that deviate from the general relativistic results at quadratic order in the Gauss-Bonnet coupling constant. We show that this result is in agreement with an analysis of unstable circular null orbits around black holes in this theory, allowing us to establish the geometrical optics–null geodesic correspondence for the axial quasinormal modes. For the polar quasinormal modes, the small-coupling approximation forces us to consider the ordering between eikonal and small-coupling perturbative parameters, one of which we show, by explicit comparison against numerical data, yields the correct identification of the quasinormal modes of the scalar-tensor coupled system of wave equations. These corrections lift the general relativistic degeneracy between scalar and tensorial eikonal quasinormal modes at quadratic order in Gauss-Bonnet coupling in a way reminiscent of the Zeeman effect. In general, our analytic, eikonal quasinormal mode frequencies (normalized to the General Relativity ones) agree with numerical results with an error of $\mathcal{O}(10\%)$ in the regime of small coupling constant. Finally, we find that the analytical expressions for the quasinormal modes are common to a broad class of scalar-Gauss-Bonnet theories to leading eikonal order, showing a degeneracy between the quasinormal modes of nonrotating black holes in particular scalar-Gauss-Bonnet theories in the geometrical optics limit.

DOI: [10.1103/PhysRevD.104.044051](https://doi.org/10.1103/PhysRevD.104.044051)

I. INTRODUCTION

The first direct observations of gravitational waves (GWs) by the LIGO/Virgo Collaborations marked the dawn of gravitational wave astronomy [1–5]. These GW events allow us to probe gravity in the strong, dynamical, and nonlinear regime [6,7] and to compare the predictions of general relativity (GR), and modifications thereof, in such extreme environments as done, e.g., in Refs. [7–13]. An example is the inspiral-merger-ringdown consistency test in a coalescing binary system [14,15]; this is a consistency check between the independent measurements of the remnant black hole’s mass and spin from the inspiral and merger-ringdown phases, assuming GR is correct. Such consistency tests can be applied beyond the realm of GR to constrain

specific theories [16] and parametrized deformed-Kerr spacetimes [17].

A similar suit of consistency tests can be performed with the ringdown signal alone, with the aim of probing the no-hair property of black holes [18]. In this approach, usually termed “black hole spectroscopy,” a measurement of the fundamental quasinormal mode (QNM) frequency and damping time allows the extraction of the remnant’s mass and spin under the assumption that the object is a garden-variety Kerr black hole. A much more powerful test—that of the Kerr hypothesis itself—can be performed if additional QNM frequencies can be observed in the data stream. Indeed, the very first event GW150914 has been analyzed in this fashion using overtones [19]. A more traditional approach is to use waveforms of the same overtone but at

different harmonics [20], which has successfully been applied recently to, e.g., GW190521 [21]. This “spectroscopic approach” can be applied to test gravity in both theory-specific [22–37] and model-independent [38–46] frameworks.

This paper makes a contribution to the former category by computing QNMs of black holes in scalar Gauss-Bonnet gravity with the help of the eikonal approximation. The action of this theory features a scalar field nonminimally coupled to the Gauss-Bonnet invariant (which itself is quadratic in curvature) [47,48]. The precise functional form of this coupling gives rise to different subtheories of gravity. For example, an exponential scalar field coupling can be identified as the Einstein-dilaton Gauss-Bonnet (EdGB) gravity motivated by string theory [49–52]. On the other hand, a linear coupling leads to a shift-symmetric theory [53–57], while theories with a quadratic coupling lead to spontaneously scalarized black holes [58–61] (this effect can also occur with other coupling functions and scalar field self-interactions; see, e.g., Refs. [62–68] for details).

In this paper, we consider the broader scalar Gauss-Bonnet gravity theory and study the QNMs of its spherically symmetric, nonrotating black holes using the eikonal approximation. We achieve this by first solving the linearized field equations describing combined scalar-tensor perturbations of black holes. The final distilled wave equations for the decoupled polar and axial degrees of freedom can be cast in a Schrödinger-like form. These equations are subsequently solved using the eikonal techniques we developed in Refs. [69,70] in the context of non-GR theories. The end result (summarized in Sec. V C) is a set of analytic eikonal formulas for the fundamental QNM’s frequency and damping time. In order to gauge the accuracy of our formulation, we consider the particular example of EdGB gravity and compare our results against the numerical QNM data computed in Ref. [25].

Figure 1 compares the (normalized) real eikonal QNM frequencies for the $\ell = 2$ harmonic in EdGB gravity against the numerical results of Ref. [25] as a function of the coupling constant α in the theory. Notice that the analytic, eikonal results match nicely with the numerical ones in the small α regime. We found that the former is accurate with an error of approximately 10%. The eikonal results become less accurate for larger α as they are derived within the small coupling approximation.

The rest of the paper is organized as follows. In Sec. II, we review the basics of scalar Gauss-Bonnet gravity and show the nonrotating black hole solution in this theory, which is then perturbed in Sec. III. Having derived the master equations governing gravito-scalar perturbations of black holes in this theory, we examine them under the lens of the eikonal limit in Sec. IV. We compare our eikonal results with the numerical ones in Sec. V and summarize the final eikonal expressions in Sec. V C. We present our

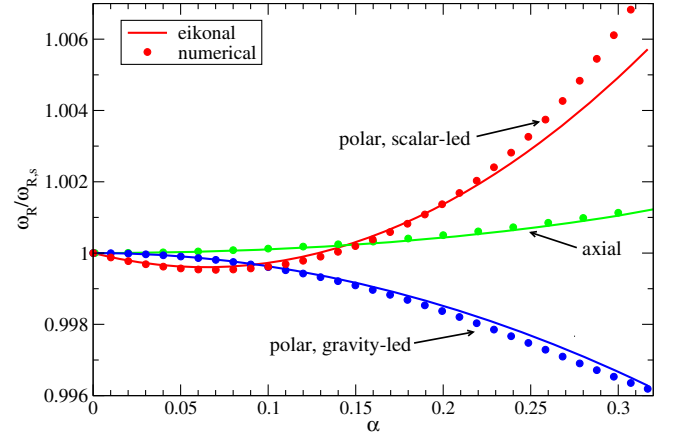


FIG. 1. Summary plot comparing eikonal and numerical real QNM frequencies (normalized by the GR Schwarzschild value) for $\ell = 2$ in EdGB gravity as a function of the coupling parameter α (in units of GR black hole mass squared). The eikonal result is computed within the small coupling approximation [valid to $\mathcal{O}(\alpha^2)$] and thus becomes more inaccurate for larger α .

conclusions in Sec. VI and give directions for potential future work. We work with geometrical units $c = G = 1$. Throughout the paper, a prime denotes a derivative with respect to a function’s argument.

II. SCALAR GAUSS-BONNET GRAVITY

We begin by reviewing the theory and a nonrotating black hole spacetime in scalar-Gauss-Bonnet gravity.

A. Theory

Our starting point is the action for scalar Gauss-Bonnet gravity [48],

$$S = \frac{1}{16\pi} \int d^4x \sqrt{-g} \left[R - \frac{1}{2} \partial_a \phi \partial^a \phi + \alpha f(\phi) \mathcal{G} \right] + S_m, \quad (2.1)$$

where

$$\mathcal{G} = R_{abcd} R^{abcd} - 4R_{ab} R^{ab} + R^2 \quad (2.2)$$

is the Gauss-Bonnet topological term and S_m is the matter part of the action. Different choices of the arbitrary scalar field function $f(\phi)$ correspond to different flavors of scalar Gauss-Bonnet theory. For example, the popular choice $f(\phi) \propto \exp(\gamma\phi)$, where γ is a constant, corresponds to EdGB gravity that arises in the low-energy limit of string theories [49–52]; $f(\phi) \propto \phi$ corresponds to shift-symmetric scalar Gauss-Bonnet theory [53–57]; the class of theories with $f(\phi) \propto \phi^2$ [58] and $f(\phi) \propto \exp(\gamma\phi^2)$ [62] has been

recently considered within the context of spontaneous scalarizations of black holes and neutron stars.

A standard variation of the action returns the field equations

$$\square\phi = \alpha f'(\phi)\mathcal{G}, \quad (2.3)$$

$$G_{ab} = \frac{1}{2}\partial_a\phi\partial_b\phi - \frac{1}{4}g_{ab}\partial_c\phi\partial^c\phi - \alpha\mathcal{K}_{ab} + 8\pi T_{ab}, \quad (2.4)$$

where G_{ab} is the usual Einstein tensor, T_{ab} is the matter stress-energy tensor, and

$$\mathcal{K}_{ab} = (g_{ac}g_{bd} + g_{ad}g_{bc})\epsilon^{ijkl}\nabla_l[*R_{jk}^{cl}\partial_i f(\phi)], \quad (2.5)$$

which arises from the Gauss-Bonnet term to the action, where ϵ^{abcd} is the Levi-Civita pseudotensor and $*R^{ab}_{cd} = \epsilon^{abij}R_{ijcd}$ is the dual to the Riemann tensor.

B. Background black hole spacetime

Nonrotating black holes in scalar Gauss-Bonnet gravity can be described by the static and spherically symmetric line element

$$g_{ab}^0 dx^a dx^b = -A(r)dt^2 + B(r)^{-1}dr^2 + r^2 d\Omega^2, \quad (2.6)$$

where $d\Omega^2$ is the unit two-sphere line element. Hereafter, we work with dimensionless quantities, i.e.,

$$r/M \rightarrow r, \quad x/M \rightarrow x, \quad \alpha/M^2 \rightarrow \alpha, \quad (2.7)$$

where M is the black hole's mass in GR. The metric functions A and B were obtained in the past, both in shift-symmetric and dilatonic flavors of scalar-Gauss-Bonnet gravity, working either perturbatively in a small α expansion around a seed Schwarzschild background black hole (see, e.g., Refs. [55,56,71,72]) or by directly integrating the field equations numerically (see, e.g., Refs. [48,51,52,58,62,73]).

Here, f is kept arbitrary for generality, but we do adopt a small coupling approximation ($\alpha \ll 1$) as done in Ref. [74]. In our coordinate system, the background metric functions A , B and scalar field ϕ_0 can be written as

$$A = 1 - \frac{2}{r} - \frac{\alpha^2 f_0'^2}{r} \left(\frac{49}{40} - \frac{1}{3r^2} - \frac{26}{3r^3} - \frac{22}{5r^4} - \frac{32}{5r^5} + \frac{80}{3r^6} \right), \quad (2.8)$$

$$B = 1 - \frac{2}{r} - \frac{\alpha^2 f_0'^2}{r} \left(\frac{49}{40} - \frac{1}{r} - \frac{1}{r^2} - \frac{52}{3r^3} - \frac{2}{r^4} - \frac{16}{5r^5} + \frac{368}{3r^6} \right), \quad (2.9)$$

$$\phi_0 = \frac{2\alpha f_0'}{r} \left(1 + \frac{1}{r} + \frac{4}{3r^2} \right) + \frac{\alpha^2 f_0' f_0''}{r} \left(\frac{73}{30} + \frac{73}{30r} + \frac{146}{45r^2} + \frac{73}{15r^3} + \frac{224}{75r^4} + \frac{16}{9r^5} \right). \quad (2.10)$$

Here, we used the shorthand notations $f'(0) = f_0'$ and $f''(0) = f_0''$. This solution represents a deformed, scalar hair-endowed Schwarzschild black hole, with deformations controlled by the parameter α . From Eq. (2.8), one finds that the Arnowitt-Deser-Misner (ADM) mass M_* of the black hole acquires an $\mathcal{O}(\alpha^2)$ correction as

$$M_* = M \left(1 + \frac{49}{80} \alpha^2 f_0'^2 \right). \quad (2.11)$$

III. BLACK HOLE PERTURBATIONS

Going beyond the background spacetime, we now analyze its stability by studying linear perturbations. We write the perturbed metric and scalar field as

$$g_{ab} = g_{ab}^0 + \bar{\epsilon} h_{ab}, \quad \phi = \phi_0 + \bar{\epsilon} \delta\phi, \quad (3.1)$$

where $\bar{\epsilon}$ is a bookkeeping parameter, while g_{ab}^0 and ϕ_0 are given by Eqs. (2.6), (2.8), (2.9), and (2.10).

Following standard techniques of black hole perturbation theory in GR [75,76], we expand the metric/scalar field perturbations into appropriate tensor/scalar harmonics basis. We work to linear order in $\bar{\epsilon}$, and after imposing the Regge-Wheeler gauge, the field equations (2.3)–(2.4) lead to a set of decouple equations for the axial and polar sectors of the perturbations. We discuss these separately in the following sections.

A. Axial perturbations

We begin by considering axial perturbations, which are decoupled from the scalar perturbations. We follow the notation of Blázquez-Salcedo *et al.* [25], where the axial perturbed metric is written as

$$h_{ab} = \begin{pmatrix} 0 & 0 & 0 & \bar{h}_0 \sin\theta \partial_\theta \\ 0 & 0 & 0 & \bar{h}_1 \sin\theta \partial_\theta \\ 0 & 0 & 0 & 0 \\ \bar{h}_0 \sin\theta \partial_\theta & \bar{h}_1 \sin\theta \partial_\theta & 0 & 0 \end{pmatrix} Y_{\ell m}, \quad (3.2)$$

where $Y_{\ell m}(\theta, \varphi)$ are the (scalar) spherical harmonics, while \bar{h}_0 and \bar{h}_1 are functions of t and r only. We can further Fourier transform these functions as

$$\bar{X}(t, r) = \frac{1}{\sqrt{2\pi}} \int d\omega X(r) e^{-i\omega t}, \quad (3.3)$$

with $X = (\bar{h}_0, \bar{h}_1)$.

Inserting Eqs. (3.2) and (3.3) into the field equations, we find two nontrivial equations for the axial gravitational perturbations. These equations, in the particular case of EdGB gravity with $f = e^\phi/4$, can be found in Appendix B of Ref. [25]. These perturbed field equations can be combined into a single equation for \bar{h}_1 and its radial derivatives. We can further make a field redefinition as

$$Q = c\bar{h}_1, \quad (3.4)$$

where $c(r)$ is found by requiring that the coefficient of the friction term $Q'(r)$ vanishes (the expression can be found in Appendix and in the supplemental *Mathematica* notebook [77]). Then, we obtain a master equation for the axial perturbation, namely

$$\frac{d^2 Q}{dx^2} + (A_{\text{ax}}\omega^2 - V_{\text{ax}})Q = 0, \quad (3.5)$$

where the tortoise coordinate x is defined as

$$x_{,r} = \frac{dx}{dr} = (AB)^{-1/2}, \quad (3.6)$$

V_{ax} is the potential for the axial perturbation, while the function A_{ax} is given by

$$A_{\text{ax}} = \frac{A}{A - 2\alpha B A' \phi'_0 f'_0} \{1 - 2\alpha B' \phi'_0 f'_0 + 4\alpha B [\phi'^2_0 f''_0 + \phi''_0 f'_0]\} \quad (3.7)$$

(where primes on A , B , and ϕ_0 refer to radial derivatives) or in the small coupling limit valid to $\mathcal{O}(\alpha^2)$,

$$A_{\text{ax}} = 1 - \frac{\alpha^2 f'^2_0}{r^3} \left(16 + \frac{16}{r} + \frac{32}{r^2} - \frac{256}{r^3}\right). \quad (3.8)$$

In the GR limit, A_{ax} reduces to unity, and Eq. (3.5) reduces to the familiar Regge-Wheeler equation. We may make yet another radial coordinate transformation

$$\frac{d\tilde{x}}{dx} = \sqrt{A_{\text{ax}}}, \quad (3.9)$$

after which Eq. (3.5) takes the form

$$\frac{d^2 Q}{d\tilde{x}^2} + p_{\text{ax}} \frac{dQ}{d\tilde{x}} + (\omega^2 - \tilde{V}_{\text{ax}})Q = 0, \quad (3.10)$$

where we have defined the friction coefficient as $p_{\text{ax}} = (A_{\text{ax}})_{,x}/(2A_{\text{ax}}^{3/2})$ and the resulting effective potential $\tilde{V}_{\text{ax}} = V_{\text{ax}}/A_{\text{ax}}$. As we will see later, the friction term

makes no contribution to the QNM frequency in the eikonal approximation. The expression for the potential $\tilde{V}_{\text{ax}}(r)$ is rather lengthy and can be found in the supplemental *Mathematica* notebook [77].

B. Polar perturbations

The polar sector of the perturbations is somewhat more complicated as a result of the coupled tensorial and scalar perturbations. The tensorial perturbations are written as [25]

$$h_{ab} = \begin{pmatrix} A\bar{H}_0 & \bar{H}_1 & 0 & 0 \\ \bar{H}_1 & \bar{H}_2/B & 0 & 0 \\ 0 & 0 & r^2\bar{K} & 0 \\ 0 & 0 & 0 & r^2 \sin^2 \theta \bar{K} \end{pmatrix} Y_{\ell m}. \quad (3.11)$$

Once again, \bar{H}_0 , \bar{H}_1 , and \bar{K} are functions of (t, r) , which we Fourier transform following Eq. (3.3). The scalar field perturbation is decomposed in a similar way as

$$\delta\phi = \frac{1}{\sqrt{2\pi}} \int dt \frac{\hat{\phi}(r)}{r} Y_{\ell m} e^{-i\omega t}. \quad (3.12)$$

Inserting these expressions in the field equations, we arrive at a system of six coupled equations [arising from Eq. (2.4)] and one from Eq. (2.3). (These equations for EdGB are shown in Ref. [25], Appendix B). Using all seven equations, we can eliminate \bar{H}_0 and \bar{H}_2 so that the remaining first-order system of differential equations takes the form [25]

$$\begin{pmatrix} \bar{H}'_1 \\ \bar{K}' \\ \hat{\phi}' \\ \hat{\phi}'' \end{pmatrix} + \begin{pmatrix} V_{11} & V_{12} & V_{13} & V_{14} \\ V_{21} & V_{22} & V_{23} & V_{24} \\ 0 & 0 & 0 & -1 \\ V_{41} & V_{42} & V_{43} & V_{44} \end{pmatrix} \begin{pmatrix} \bar{H}_1 \\ K \\ \hat{\phi} \\ \hat{\phi}' \end{pmatrix} = \begin{pmatrix} 0 \\ 0 \\ 0 \\ 0 \end{pmatrix}. \quad (3.13)$$

Following the original treatment by Zerilli [76], the two first-order gravitational perturbation equations may be rewritten as a single second-order differential equation. By means of the field redefinitions

$$\bar{K}(r) = g(r)\hat{K}(r) + \hat{R}(r), \quad (3.14)$$

$$\bar{H}_1(r) = \omega(h(r)\hat{K}(r) + k(r)\hat{R}(r)), \quad (3.15)$$

choosing g , h , and k such that

$$\frac{d\hat{K}}{dx} = \hat{R}, \quad (3.16)$$

$$\frac{d\hat{R}}{dx} = [A_0 + A_2\omega^2]\hat{K}, \quad (3.17)$$

we obtain an inhomogeneous Schrödinger-type equation for \hat{K} , the non-GR source term of that equation depends on ω , $\hat{\phi}$, and $\hat{\phi}'$. The functions $A_0(r)$ and $A_2(r)$ originate from the field redefinitions (3.14) and (3.15).

The final distilled form of the polar perturbation equations is a system of two coupled wave equations,

$$\frac{d^2\hat{K}}{dx^2} + p_{\text{pol}} \frac{d\hat{K}}{dx} + (A_{\text{pol}}\omega^2 - V_{\text{pol}})\hat{K} = a_0\hat{\phi} + a_1 \frac{d\hat{\phi}}{dx}, \quad (3.18)$$

$$\frac{d^2\hat{\phi}}{dx^2} + (\omega^2 - V_{\phi})\hat{\phi} = b_0\hat{K} + b_1 \frac{d\hat{K}}{dx}. \quad (3.19)$$

Here p_{pol} , A_{pol} , a_0 , a_1 , b_0 , and b_1 are functions of r whose explicit forms in the small coupling approximation are given in Appendix and the supplemental *Mathematica* notebook [77]. The potential V_{pol} for the gravitational perturbation equation is given, also in the small coupling approximation, as

$$V_{\text{pol}}(r) = V_Z(r) + V_2(r)\alpha^2 f_0'^2. \quad (3.20)$$

Here, V_Z is the Zerilli potential [76]

$$V_Z = \left(1 - \frac{2}{r}\right) \frac{2\Lambda^2(\Lambda + 1)r^3 + 6\Lambda^2 r^2 + 18\Lambda r + 18}{r^3(\Lambda r + 3)^2}, \quad (3.21)$$

with

$$\Lambda = (\ell + 2)(\ell - 1)/2, \quad (3.22)$$

while V_2 and the scalar perturbation potential V_{ϕ} [appearing in Eq. (3.19)] are given in Appendix and the supplemental *Mathematica* notebook [77]. Taking the GR limit ($\alpha \rightarrow 0$) removes all the right-hand side coupling terms in Eqs. (3.18) and (3.19) and reduces the left-hand sides to the Zerilli and free scalar field wave equations, respectively. Note that the system, Eqs. (3.18) and (3.19), does not belong to the general family of coupled equations studied in Refs. [69,70].

IV. EIKONAL QNMS

Having obtained the equations governing axial (3.5) and polar (3.18)–(3.19) perturbations in scalar Gauss-Bonnet gravity, we now proceed to analyze their QNM spectra in

the eikonal limit using the methods developed in the previous papers of the series [69,70].

A. Axial QNMs

We start off with the axial sector, which provides a simple setup to review these methods. Here, we use coordinates given by Eqs. (3.6) and (3.9), which may be expressed in the small coupling limit as

$$\tilde{x}, r = \left(1 - \frac{2}{r}\right)^{-1} \left[1 + \frac{\alpha^2 f_0'^2}{r} \left(\frac{49}{40} + \frac{39}{20r} - \frac{143}{30r^2} - \frac{218}{15r^3} - \frac{484}{15r^4} - \frac{272}{3r^5} \right) \right]. \quad (4.1)$$

The eikonal prescription is based on a phase-amplitude solution of the form

$$Q(\tilde{x}) = \mathcal{A}_Q(\tilde{x}) e^{iS(\tilde{x})/\epsilon}, \quad (4.2)$$

where ϵ is the eikonal bookkeeping parameter. The eikonal limit corresponds to $\epsilon \ll 1$ and $\ell \gg 1$, while keeping the balance $\epsilon\ell = \mathcal{O}(1)$. For later convenience, we decompose the potential into

$$\tilde{V}_{\text{ax}} = \ell(\ell + 1)V_{\text{ax}1} + V_{\text{ax}2}, \quad (4.3)$$

where $V_{\text{ax}1}$ and $V_{\text{ax}2}$ are independent of both ℓ and ω ; thus, only the former function can contribute to the QNM spectra in the eikonal limit.

1. Leading-order analysis

Substituting the ansatz (4.2) into Eq. (3.10), we find the following leading-order eikonal equation:

$$-\frac{(S_{,\tilde{x}})^2}{\epsilon^2} + \omega^2 - \ell^2 V_{\text{ax}1} = 0. \quad (4.4)$$

The explicit expression for the effective potential $V_{\text{ax}1}$ vanishes for arbitrarily large $|\tilde{x}|$ with a peak, located at a radial position denoted r_m , where $V'_{\text{ax}1}(r_m) = (V'_{\text{ax}1})_m = 0$. The derivative of Eq. (4.4) evaluated at r_m yields

$$\frac{2}{\epsilon^2} (S_{,\tilde{x}})_m (S_{,\tilde{x}\tilde{x}})_m = -\ell^2 \left(\frac{dr}{d\tilde{x}} \right)_m (V'_{\text{ax}1})_m = 0, \quad (4.5)$$

showing the potential is the extremum at the same location where $S_{,\tilde{x}} = 0$ given $S_{,\tilde{x}\tilde{x}} \neq 0$. A location of stationary phase S follows from imposing purely ingoing and outgoing plane wave solutions as $|\tilde{x}| \gg 0$, that is, purely ingoing toward the horizon and purely outgoing at spatial infinity, requiring a minimum $S_{,\tilde{x}} = 0$ already determined by Eq. (4.5). Hence, Eq. (4.4) at this peak yields

$$\omega^2 = \ell^2 (V_{\text{ax}1})_m, \quad (4.6)$$

given explicitly by

$$\omega_R^{(0)} = \ell \left[\frac{A - 2\alpha B A' \phi'_0 f'_0}{r(r - 4\alpha B \phi'_0 f'_0)} \right]_m^{1/2}, \quad (4.7)$$

where the labels denote that this is the leading-order real part of the QNM modes.

The condition $V_{\text{ax}1,r} = 0$ becomes

$$(r_m - 3) - \alpha^2 f_0'^2 \left(\frac{147}{80} + \frac{155}{6r_m^2} - \frac{98}{r_m^3} - \frac{77}{5r_m^4} - \frac{1408}{5r_m^5} + \frac{984}{r_m^6} \right) = 0 \quad (4.8)$$

and may be solved for r_m by means of a small coupling expansion ansatz. Solving to second order, we obtain

$$r_m = 3 + \frac{6577}{19440} \alpha^2 f_0'^2, \quad (4.9)$$

where the first term represents the GR photon ring i.e., the radius of the unstable photon circular orbit.

Hence, the leading-order real mode can be expressed as

$$\omega_R^{(0)} = \frac{\ell}{3\sqrt{3}} \left(1 - \frac{71987}{174960} \alpha^2 f_0'^2 \right), \quad (4.10)$$

where we can again identify the first term as the appropriate GR limit.

2. Subleading-order analysis

Let us next derive the QNM frequency at the subleading eikonal order. The subleading order equation evaluated at the potential peak gives

$$\frac{i(S_{,\tilde{x}\tilde{x}})_m}{\epsilon} - \ell(V_{\text{ax}1})_m + 2(\omega_R^{(1)} + i\omega_I^{(1)})\omega_R^{(0)} = 0, \quad (4.11)$$

where we used

$$\omega = \omega_R^{(0)} + \epsilon(\omega_R^{(1)} + i\omega_I^{(1)}) + \mathcal{O}(\epsilon^2). \quad (4.12)$$

Taking the real part of Eq. (4.11) and using Eq. (4.7), we find the subleading eikonal correction to the real part of the axial QNM frequency as

$$\omega_R^{(1)} = \frac{1}{2} \left[\frac{A - 2\alpha B A' \phi'_0 f'_0}{r(r - 4\alpha B \phi'_0 f'_0)} \right]_m^{1/2} = \frac{\omega_R^{(0)}}{2\ell}. \quad (4.13)$$

We can combine this expression with the leading-order result to obtain

$$\begin{aligned} \omega_R &= \omega_R^{(0)} + \epsilon\omega_R^{(1)}, \\ &= \left(\ell + \frac{\epsilon}{2} \right) \left[\frac{A - 2\alpha B A' \phi'_0 f'_0}{r(r - 4\alpha B \phi'_0 f'_0)} \right]_m^{1/2}. \end{aligned} \quad (4.14)$$

Finally, using Eq. (4.9) and the background solutions, we find

$$\omega_R = \frac{1}{3\sqrt{3}} \left(\ell + \frac{\epsilon}{2} \right) \left(1 - \frac{71987}{174960} \alpha^2 f_0'^2 \right). \quad (4.15)$$

Let us now derive the imaginary part. To do so, we need $(S_{,\tilde{x}\tilde{x}})_m$, which can be solved for by doing a Taylor expansion of the leading-order equation (4.4) around r_m with ω given by Eq. (4.7), followed by a derivative with respect to \tilde{x} . These steps result in

$$\frac{S_{,\tilde{x}\tilde{x}}^2}{\epsilon^2} \approx -\frac{\ell^2}{2} (V''_{\text{ax}1})_m (\tilde{x} - \tilde{x}_m)^2. \quad (4.16)$$

A Taylor expansion of the left-hand-side term about the peak radius leads to

$$\frac{(S_{,\tilde{x}\tilde{x}})_m}{\epsilon} = \frac{\ell}{\sqrt{2}x_{,r}} |V''_{\text{ax}1}|_m^{1/2}. \quad (4.17)$$

Finally, substituting Eq. (4.17) in Eq. (4.11) gives

$$\omega_I = \epsilon\omega_I^{(1)} = -\frac{1}{2(\tilde{x}_{,r})_m} \sqrt{\frac{|V''_{\text{ax}1}|}{2V_{\text{ax}1}}}_m. \quad (4.18)$$

Using Eq. (4.9) further, we obtain

$$\begin{aligned} \omega_I &= -\frac{\epsilon}{2\sqrt{3}(\tilde{x}_{,r})_m} \left(1 - \frac{115771}{174960} \alpha^2 f_0'^2 \right), \\ &= -\frac{\epsilon}{6\sqrt{3}} \left(1 - \frac{121907}{174960} \alpha^2 f_0'^2 \right), \end{aligned} \quad (4.19)$$

which also recovers the well-known GR limit.

3. Comparison with geodesic correspondence

In Ref. [25], approximate QNM frequencies for axial modes were computed from the null geodesic correspondence in the eikonal limit [78–80] and were compared with numerical results. We compare here our eikonal calculations with the geodesic correspondence results.

The geodesic correspondence allows one to compute QNM frequencies only from properties of the photon ring. The complex QNM frequency under this correspondence is related to the metric functions as [79]

$$\omega^{(\text{geod})} = \ell \frac{\sqrt{A(r_c)}}{r_c} - i \frac{r_c}{2\sqrt{2}} \sqrt{-\frac{1}{A(r_c)} \left(\frac{d^2 A}{d\tilde{x}^2 r^2} \right)_{r=r_c}}, \quad (4.20)$$

where r_c is the location of the photon ring determined from the equation

$$2A(r_c) = r_c A'(r_c). \quad (4.21)$$

For scalar-Gauss-Bonnet gravity and in the small coupling approximation, we can use Eq. (2.8) and solve this equation for r_c order by order in α to find

$$r_c = 3 + \frac{4219}{6480} \alpha^2 f_0'^2, \quad (4.22)$$

to second order in α .

Let us first study the real part of the QNM frequency

$$\omega_R^{(\text{geod})} = \ell \frac{\sqrt{A(r_c)}}{r_c}. \quad (4.23)$$

From Eqs. (2.8) and (4.22), we find

$$\omega_R^{(\text{geod})} = \frac{\ell}{3\sqrt{3}} \left(1 - \frac{71987}{174960} \alpha^2 f_0'^2 \right). \quad (4.24)$$

Notice that this is exactly the same as $\omega_R^{(0)}$ in Eq. (4.10) obtained from the eikonal calculation. At a first glance, this seems a bit surprising since Eq. (4.7) contains the scalar field dependence whereas Eq. (4.23) does not, and the right-hand side of the former equation is evaluated at r_m , which is different from r_c .

The apparent difference in the real part of the QNM frequency in the two analyses mentioned above does not affect the final expression under the small coupling approximation for the following reason. First, let us look at the two terms in Eq. (4.7) that involve the scalar field ϕ_0 . Given that these are already multiplied by α and $\phi_0 = \mathcal{O}(\alpha)$, we can replace $A' \rightarrow A'_{\text{GR}} = d(1 - 2/r)/dr = 2/r^2$, $B \rightarrow B_{\text{GR}} = 1 - 2/r$, $\phi'_0 \rightarrow \alpha \phi'_1$ and $f'(\phi_0) \rightarrow f'_0$ if we only work up to $\mathcal{O}(\alpha^2)$, where the subscript “GR” denotes the GR contribution and ϕ_1 is the $\mathcal{O}(\alpha)$ piece in ϕ_0 (with α being factored out). Replacing further $A \rightarrow A_{\text{GR}} + \alpha^2 \delta A$ and $r_m \rightarrow 3 + \alpha^2 \delta r_m$ with δA and δr_m being some generic functions that are independent of α , we find

$$\begin{aligned} \omega_R^{(0)} &= \ell \left[\frac{A_{\text{GR}} + \alpha^2 \delta A - 2\alpha^2 B_{\text{GR}} A'_{\text{GR}} \phi'_1 f'_0}{r(r - 4\alpha^2 B_{\text{GR}} \phi'_1 f'_0)} \right]^{1/2}_{r=3+\delta r_m} \\ &\approx \frac{\ell}{3\sqrt{3}} \left(1 + \frac{3}{2} \alpha^2 \delta A(3) \right). \end{aligned} \quad (4.25)$$

Notice that the GB correction only depends on δA and is independent of ϕ_1 and δr_m . Also notice that we only need to evaluate δA at the GR value for r_m , namely $r = 3$. Substituting in $\delta A(3) = -71987 f_0'^2 / 262440$, we recover Eq. (4.10). The above calculation proves analytically that the scalar field (and also δr_m) dependence in Eq. (4.7) cancels at $\mathcal{O}(\alpha^2)$, leading to the same expression for the real QNM frequency as in the geodesic correspondence.

Next, we study the imaginary part of the QNM frequency in the geodesic side of the correspondence. From

Eq. (4.20), together with Eqs. (2.8), (2.9), and (4.22), we find to $\mathcal{O}(\alpha^2)$

$$\begin{aligned} \omega_I^{(\text{geod})} &= -\frac{r_c}{2\sqrt{2}} \sqrt{-\frac{1}{A(r_c)} \left(\frac{d^2 A}{d\tilde{x}^2 r^2} \right)_{r=r_c}}, \\ &\approx -\frac{1}{6\sqrt{3}} \left(1 - \frac{121907}{174960} \alpha^2 f_0'^2 \right). \end{aligned} \quad (4.26)$$

Once again, this is same as the eikonal result in Eq. (4.19). In conclusion, our eikonal QNM calculation agree with those from the geodesic correspondence up to $\mathcal{O}(\alpha^2)$ for the axial modes.

B. Polar QNMs

Let us next study the eikonal QNM frequencies in the polar sector. The coupled wave equations describing polar QNMs are given in Eqs. (3.18) and (3.19) valid to $\mathcal{O}(\alpha^2)$. As we did in the axial case, we start by introducing the eikonal ansatz,

$$\hat{K}(x) = \mathcal{A}_K(x) e^{iS(x)/\epsilon}, \quad \hat{\phi}(x) = \mathcal{A}_\phi(x) e^{iS(x)/\epsilon}. \quad (4.27)$$

Note that both fields share the same phase function S (this should not be confused with the previous axial phase function). As already pointed out, we assume an eikonal scaling $\ell = \mathcal{O}(\epsilon)$, which is appropriate for standard “Price” QNMs. Similar to the axial case, the leading-order frequency of these modes is ω_R , while ω_I first appears at subleading order.

On paper, the strategy for manipulating the wave equations should be simple: after using Eq. (4.27), we solve the tensorial equation for \mathcal{A}_ϕ and then insert the result in the scalar equation. The outcome is an algebraic biquadratic equation for ω , which is supposed to be solved at the peak radius $r = r_m$ (once again, not to be confused with the peak location for the axial potential) of an effective potential similar to Eq. (40) of Ref. [69]. In the previous papers of this series [69,70], the $\epsilon \rightarrow 0$ limit was applied to this equation (or equivalently to its solutions), resulting in eikonal expressions for ω (up to a specified order). Taking the eikonal limit in the present analysis requires a more subtle computation due to the presence of a second small parameter in the system, the coupling constant α . The polar calculation is essentially a biparametric expansion in $\epsilon \ll 1$ and $\alpha \ll 1$, and one has to make a prior decision as to whether α/ϵ is supposed to be a small or a large parameter. This is a necessary step because, as we show below, taking the eikonal limit before expanding in α is *not* equivalent to the same limits taken in the reverse order.

The equation for ω can be symbolically written as

$$\omega^4 + F(\epsilon, \alpha, \ell, r_m, Q_m) \omega^2 + G(\epsilon, \alpha, \ell, r_m, Q_m) = 0, \quad (4.28)$$

where F and G are rational functions of their arguments and $Q = \{S'', \mathcal{A}_K, \mathcal{A}'_K, \mathcal{A}''_\phi, \mathcal{A}'_\phi, \mathcal{A}''_\phi\}$, where primes now represent x derivatives. In the double limit $\epsilon = \alpha = 0$, this equation reduces to

$$\left[\omega^2 - \frac{\ell^2}{r_m^2} \left(1 - \frac{2}{r_m} \right) \right]^2 = 0, \quad (4.29)$$

with the familiar GR double root $\omega_{\text{GR}}^2 = \ell^2/27$ (with $r_m = 3$) for gravitational and scalar perturbations.

We now solve Eq. (4.28) for nonvanishing values of ϵ , α in combination with the ansatz for the peak location given by

$$\omega_{\pm}^2 = \frac{\ell^2}{27} \left\{ 1 + \frac{\epsilon}{\ell} \left(1 - \frac{27i}{\ell} S''_m \right) \pm \frac{8}{9} f'_0 \alpha \left[1 + \frac{\epsilon}{\ell} \left(1 - \frac{4i}{\ell} S''_m \right) \right] - \frac{\alpha^2}{3} \left[\frac{67307}{58320} f_0'^2 \mp \frac{320}{243} f'_0 f''_0 \right] \right\} + \mathcal{O}(\alpha^3, \epsilon^2, \alpha^2 \epsilon). \quad (4.32)$$

Among other things, these display a characteristic linear α -dependence at leading eikonal order. This is not too surprising, given that both functions F and G in Eq. (4.28) contain linear- α terms.

The second approach is that of “eikonal limit after small- α expansion” (which amounts to $\alpha \ll \epsilon$). Application of this algorithm [together with Eq. (4.30)] to the roots of Eq. (4.28) leads to

$$\omega_{\pm}^2 = \frac{\ell^2}{27} \left\{ 1 + \frac{\epsilon}{\ell} \left(1 - 27i \frac{S''_m}{\ell} \right) \pm \frac{8\alpha^2 f_0'^2}{27\epsilon} \left[\frac{\ell^2}{\epsilon} + 2(\ell - 4i S''_m) \right] \right\} + \mathcal{O}(\alpha^3, \epsilon^2). \quad (4.33)$$

This new pair of roots is clearly not the same as the one obtained earlier; the most striking difference is the absence of a linear- α leading-order correction and the unconventional eikonal scaling of the $\mathcal{O}(\alpha^2)$ piece. The linear correction first appears at $\mathcal{O}(\epsilon^2)$ and is therefore omitted in Eq. (4.33). Although terms scaling as approximately $\epsilon^{-2}, \epsilon^{-1}$ are formally of leading eikonal order, the fact that they appear together with α^2 effectively reduces their perturbative order and makes them smaller than the first GR term. This is equivalent to saying that $\alpha \ll \epsilon$, i.e., the opposite arrangement to that of the first approach. Another difference is the absence of f_0'' terms in Eq. (4.33) relative to Eq. (4.32). This says that modulo a trivial rescaling of the coupling constant the second approach predicts a “theory degeneracy” between shift-symmetric and dilatonic scalar-Gauss-Bonnet theories whose f_0' expressions differ by a constant at most. As we will see later, an f_0'' dependence does exist, but only at higher eikonal orders.

Which of these two nonequivalent approaches should we trust? The fact that we are looking for QNMs with a smooth GR limit suggests that $\alpha \ll \epsilon$ (i.e., the second

$$r_m = 3 + \epsilon r_{01} + \alpha(r_{10} + \epsilon r_{11}) + \alpha^2(r_{20} + \epsilon r_{21}). \quad (4.30)$$

We can proceed following the same recipe as in the axial case, finding that $r_{10} = r_{01} = 0$ and

$$r_{20} = -\frac{32 f_0'^2 \ell \alpha^2}{27 \epsilon}. \quad (4.31)$$

Unlike the others, this contribution to the peak location will be required in the S''_m calculation later.

Our first approach is that of “eikonal limit before small- α expansion” (which amounts to $\epsilon \ll \alpha$). We find the pair of roots,

approach) is the appropriate ordering of small parameters. As we discuss below, this choice is also the one in agreement with the numerical QNM data of Ref. [25]. Taking the square root of Eq. (4.33), we obtain the following solutions for the real and imaginary parts of ω up to subleading eikonal order:

$$\omega_{R\pm} = \frac{\ell}{3\sqrt{3}} \left[1 + \frac{\epsilon}{2\ell} \pm \frac{4}{27} \frac{\alpha^2 \ell^2 f_0'^2}{\epsilon^2} \left(1 + \frac{3\epsilon}{2\ell} \right) \right], \quad (4.34)$$

$$\omega_{I\pm} = -\frac{3\sqrt{3}\epsilon}{2\ell} \left(1 \mp \frac{44}{729} \frac{\alpha^2 \ell^2 f_0'^2}{\epsilon^2} \right) S''_m. \quad (4.35)$$

The coupled character of the wave equations could in principle allow for exotic QNMs whose leading-order eikonal part is dominated by non-GR terms. Such modes would have no GR counterpart and would become trivial solutions $\omega \rightarrow 0$ in the $\alpha \rightarrow 0$ limit. We have not been able to find any QNMs with this property (nor do they appear in the numerical analysis of Ref. [25]).

The above expressions capture the modifications to the well-known GR eikonal expression $\omega_s = (\ell + 1/2 + i/2)/(3\sqrt{3})$ for the massless scalar and gravitational QNM frequencies of a Schwarzschild black hole. We see that the α^2 -corrections break the degeneracy between the eikonal QNMs of these two degrees of freedom. The splitting is symmetric, reminiscent of the Zeeman effect. (The same symmetric splitting of modes can also be caused by leading-order corrections in spin to the QNMs of a Schwarzschild black hole).

The missing ingredient to calculate $\omega_{I\pm}$ is an expression for S''_m . This result can be obtained through the same steps as done for the axial perturbations, with the final result being

$$S_m'' = \frac{\ell}{27} \left(1 - \frac{560}{2187} \frac{\alpha^2 \ell^2 f_0'^2}{\epsilon} \right). \quad (4.36)$$

Substituting this expression in Eq. (4.35) gives the final result for the imaginary part of ω ,

$$\omega_{I\pm} = -\frac{\epsilon}{6\sqrt{3}} \left(1 \pm \frac{44}{729} \frac{\alpha^2 \ell^2 f_0'^2}{\epsilon^2} \right). \quad (4.37)$$

V. COMPARISON AGAINST NUMERICAL RESULTS

Let us now compare the eikonal QNM frequencies with the ones found numerically in EdGB gravity in Ref. [25]. In this subsection, we use $f = \exp(\phi)/4$ and thus $f_0' = 1/4$.

A. Axial modes

Let us begin with the axial modes. Our results for the QNM frequencies obtained in the previous section were expressed in terms of the bare Schwarzschild mass M . These can be rewritten in terms of the observable ADM mass M_* using Eq. (2.11). [The shift $M \rightarrow M_*$ introduces $\mathcal{O}(\alpha^2)$ corrections and therefore does not affect the normalized coupling constant.] For the axial mode, we find

$$\omega_R = \left(\ell + \frac{\epsilon}{2} \right) \frac{1}{3\sqrt{3}M_*} \left(1 + \frac{4397}{21870} \alpha^2 f_0'^2 \right), \quad (5.1)$$

$$\omega_I = -\frac{\epsilon}{6\sqrt{3}M_*} \left(1 - \frac{1843}{21870} \alpha^2 f_0'^2 \right). \quad (5.2)$$

The top panel of Fig. 2 presents the real and imaginary axial QNM frequencies normalized by the Schwarzschild case in GR (ω_s) as a function of α . We compare the analytic eikonal results with numerical ones. The bottom panel shows the absolute fractional difference defined as

$$\begin{aligned} (\text{abs. frac. diff.}) &= \left| \frac{[(\omega/\omega_s)_{\text{eik}} - 1] - [(\omega/\omega_s)_{\text{num}} - 1]}{(\omega/\omega_s)_{\text{num}} - 1} \right| \\ &= \left| \frac{(\omega/\omega_s)_{\text{eik}} - (\omega/\omega_s)_{\text{num}}}{(\omega/\omega_s)_{\text{num}} - 1} \right|. \end{aligned} \quad (5.3)$$

Namely, it measures the difference in the deviation of each curve from unity. For the real frequency, the eikonal calculation provides an accurate estimate within an error of approximately 10% (once the GR frequency has been corrected to the true value). For the imaginary frequency, the eikonal calculation is slightly worse and an error of approximately 40% for $\alpha \lesssim 0.5$. The eikonal calculation breaks down for large α since it is only valid to $\mathcal{O}(\alpha^2)$. We note that for non-normalized, raw frequencies, the real (imaginary) eikonal result has an error of 3% (8%) in GR.

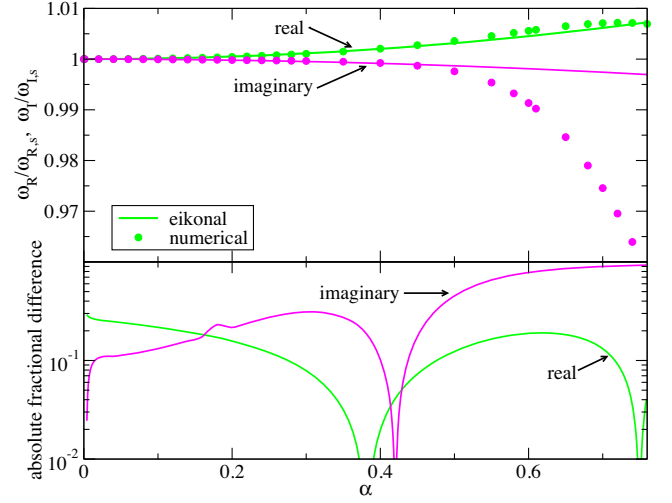


FIG. 2. Top: real and imaginary axial QNM frequencies from eikonal [cf. Eqs. (5.1) and (5.2)] and numerical results in EdGB gravity normalized by the corresponding Schwarzschild case in GR with $\alpha = 0$ ($\omega_{R,s}$ and $\omega_{I,s}$). Bottom: absolute fractional difference in Eq. (5.3) between the eikonal and the numerical results.

B. Polar modes

Let us next look at the polar modes. We present real and imaginary frequency results in turn.

1. Real frequency

We begin by keeping only the leading eikonal corrections. When $\epsilon \ll \alpha$, the real QNM frequency can be computed from Eq. (4.32), which is given in terms of the Schwarzschild mass M (which has been set to 1). When converting this to the ADM mass M_* , one finds

$$\omega_{R\pm}^{(\epsilon \ll \alpha)} = \frac{\ell}{3\sqrt{3}M_*} \left(1 \pm \frac{4}{9} \alpha f_0' + \frac{112459 f_0' \pm 76800 f_0''}{349920} \alpha^2 f_0' \right). \quad (5.4)$$

On the other hand, when $\alpha \ll \epsilon$, the real part of the QNM frequency to leading eikonal order and to leading scalar-Gauss-Bonnet correction is given by Eq. (4.34). The scalar-Gauss-Bonnet correction to the mass enters at $\mathcal{O}(\epsilon^0)$, which is of higher order than the $\mathcal{O}(\epsilon^{-2})$ above and thus can be neglected to leading order:

$$\omega_{R\pm}^{(\alpha \ll \epsilon)} = \frac{\ell}{3\sqrt{3}M_*} \left(1 \pm \frac{4}{27} \frac{\alpha^2 \ell^2 f_0'^2}{\epsilon^2} \right). \quad (5.5)$$

The top panel of Fig. 3 presents the comparison between the above eikonal calculations and numerical results found in Ref. [25]. Notice that the gravitational modes found numerically agree well with the eikonal “negative” mode within the assumption $\alpha \ll \epsilon$. On the other hand, the eikonal “positive” mode with $\alpha \ll \epsilon$ does not agree well

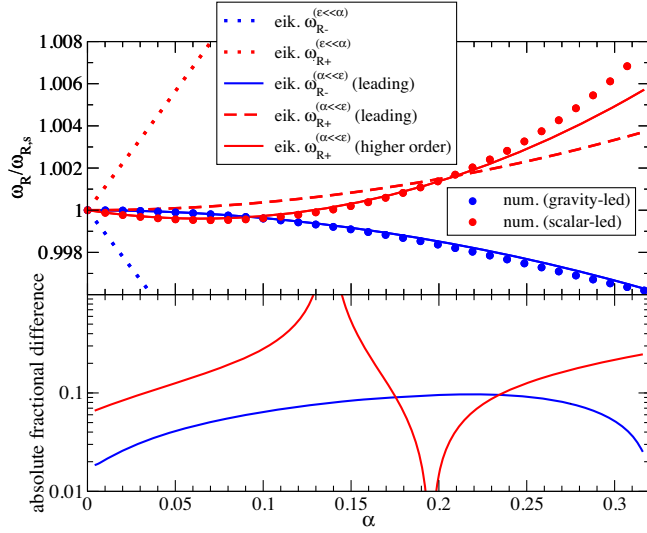


FIG. 3. Top: normalized real QNM frequencies for the $\ell = 2$ polar modes in EdGB gravity. We compare the leading eikonal calculations [cf. Eqs. (5.4) and (5.5)] and those with higher eikonal contribution for the $+$ mode [cf. Eq. (5.7)] with numerical ones. Bottom: absolute fractional difference in Eq. (5.3) between eikonal and numerical calculations. The large difference at $\alpha \sim 0.13$ is an artifact of the numerical value crossing $\omega_R/\omega_{R,s} = 1$.

with the numerical scalar-led mode. Furthermore, the eikonal calculations with $\epsilon \ll \alpha$ deviate significantly from the numerical results. This is because of a relatively large numerical coefficient at $\mathcal{O}(\alpha)$ in Eq. (5.4).

How can we make the eikonal positive mode agree better with the numerical scalar-led mode? The numerical result has a minimum at $\alpha \sim 0.08$, which cannot be realized by the eikonal leading result in Eq. (5.5) since it is monotonically increasing in α . To overcome this, one can take into account higher-order contributions in the eikonal expansion. We found that $\mathcal{O}(\alpha)$ contribution enters at $\mathcal{O}(\epsilon^2)$ in ω_+^2 in Eq. (4.33). Keeping only the real contribution, we find¹

$$(\omega_{R+}^{(\alpha \ll \epsilon)})^2 = \frac{1}{27} \left[\ell^2 + \epsilon \ell + \frac{2}{3} \epsilon^2 - \frac{16}{27} \alpha \epsilon^2 f_0'' + \frac{8}{27} \frac{\alpha^2}{\epsilon^2} \ell^2 \left(\ell^2 + 2\epsilon \ell + \frac{4}{3} \epsilon^2 \right) f_0'^2 \right], \quad (5.6)$$

where we neglected a term proportional to \mathcal{A}_K'' as such terms are unknown within the eikonal framework. Since we found there are no real corrections at $\mathcal{O}(\alpha \epsilon^3)$ while the one at $\mathcal{O}(\alpha \epsilon^4)$ is proportional to \mathcal{A}_K'' that we neglect, the above expression corresponds to keeping up to next-to-next-to-leading eikonal contributions at *each order* in α . We found that the contribution of the term at $\mathcal{O}(\alpha^0 \epsilon^2)$ is negligible, and thus we do not consider it from here on. We further

¹The imaginary part of ω^2 contributes to ω_{R+} at $\mathcal{O}(\alpha^2 \epsilon^0)$, which we do not consider for simplicity.

convert the mass to the ADM mass M_* , take a square root, expand about $\alpha = 0$, and keep up to $\mathcal{O}(\alpha^2)$ to find²

$$\omega_{R+}^{(\alpha \ll \epsilon)} = \frac{\sqrt{\ell(\ell + \epsilon)}}{3\sqrt{3}M_*} \left\{ 1 - \frac{8\alpha\epsilon^2}{27\ell(\ell + \epsilon)} f_0'' + \frac{4}{27} \frac{\alpha^2 f_0'^2}{\epsilon^2(\ell + \epsilon)} \times \left[\ell^2(\ell + 2\epsilon) + \frac{4}{3} \ell \epsilon^2 + \frac{1323}{320} \epsilon^2(\ell + \epsilon) \right] \right\}. \quad (5.7)$$

Notice that the frequency now has a f_0'' dependence that was absent in the expression to leading eikonal order. We present this result in the top panel of Fig. 3. Notice that the agreement with the numerical result has been improved.

The bottom panel of Fig. 3 presents the absolute fractional difference of selected eikonal estimate from the numerical values. For the gravity-led mode, the numerical result is recovered with an error smaller than 10%. For the scalar-led mode, the eikonal result including higher-order contribution also reproduces the numerical result with an error of 20% or smaller in the most range of $\alpha < 0.3$. The eikonal result becomes less accurate for larger α as it is obtained within the small coupling approximation. An apparent large deviation around $\alpha \sim 0.13$ is an artifact of the numerical value crossing $\omega_R/\omega_{R,s} = 1$.

2. Imaginary frequency

We now compare the imaginary part of the eikonal polar frequency with numerical results. Similar to the real frequency case, ω_I with $\epsilon \ll \alpha$ does not reproduce the numerical data, so we focus on $\alpha \ll \epsilon$ given in Eq. (4.37). Since the correction to the ADM mass is of higher eikonal order than the one in Eq. (4.37) and can be neglected, we can simply multiply the expression in Eq. (4.37) by $1/M_*$ to find the expression in the ADM mass.

Figure 4 compares the analytic eikonal results to the numerical ones. The $+$ ($-$) mode monotonically decreases (increases) in terms of α , which is similar to the scalar-led (gravity-led) modes. However, the agreement between the two is not as good as the real frequency case. We have also tried including next-to-leading eikonal contributions, but they did not improve the analytic results much. Unlike the real frequency case, the contribution at $\mathcal{O}(\alpha)$ is proportional to \mathcal{A}_ϕ'' , which is unknown in the eikonal framework. This may be one of the reasons why the eikonal results are less accurate for the imaginary frequency than the real one.

C. Summary of eikonal QNM frequencies

We summarize here the final expressions for the eikonal QNM frequencies.

²We ignored a term at $\mathcal{O}(\alpha^2 \epsilon^4)$ that is unimportant.

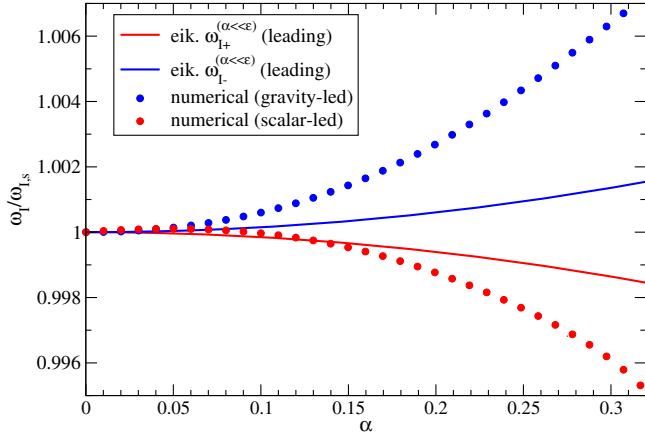


FIG. 4. Normalized imaginary polar QNM frequencies for the + and − modes for $\ell = 2$ in EdGB gravity. We compare the leading eikonal results given by Eq. (4.37) with the numerical ones.

1. Axial

For axial modes, the real and imaginary eikonal frequencies are given by Eqs. (5.1) and (5.2):

$$\omega_R = \left(\ell + \frac{\epsilon}{2}\right) \frac{1}{3\sqrt{3}M_*} \left(1 + \frac{4397}{21870} \alpha^2 f_0'^2\right), \quad (5.8)$$

$$\omega_I = -\frac{\epsilon}{6\sqrt{3}M_*} \left(1 - \frac{1843}{21870} \alpha^2 f_0'^2\right). \quad (5.9)$$

2. Polar

For the polar modes and in the $\alpha \ll \epsilon$ limit, the real eikonal frequencies for the gravity- and scalar-led modes are given, respectively, by Eqs. (5.5) and (5.7):

$$\omega_{R-} = \frac{\ell}{3\sqrt{3}M_*} \left(1 - \frac{4}{27} \frac{\alpha^2 \ell^4 f_0'^2}{\epsilon^2}\right), \quad (5.10)$$

$$\omega_{R+} = \frac{\sqrt{\ell(\ell + \epsilon)}}{3\sqrt{3}M_*} \left\{ 1 - \frac{8\alpha\epsilon^2}{27\ell(\ell + \epsilon)} f_0'' + \frac{4}{27} \frac{\alpha^2 f_0'^2}{\epsilon^2(\ell + \epsilon)} \right. \\ \left. \times \left[\ell^2(\ell + 2\epsilon) + \frac{4}{3} \ell \epsilon^2 + \frac{1323}{320} \epsilon^2(\ell + \epsilon) \right] \right\}. \quad (5.11)$$

For the imaginary part, the leading eikonal result is given in Eq. (4.37) multiplied by $1/M_*$:

$$\omega_{I\pm} = -\frac{\epsilon}{6\sqrt{3}M_*} \left(1 \pm \frac{44}{729} \frac{\alpha^2 \ell^2 f_0''}{\epsilon^2}\right). \quad (5.12)$$

VI. CONCLUSIONS

As a follow-up to our previous work [69,70], in this paper, we have studied the perturbations of nonrotating black holes in scalar Gauss-Bonnet gravity within a small-coupling approximation and have calculated the fundamental QNM frequencies in the eikonal/geometric optics approximation.

We first showed how the initial—and rather complicated—coupled perturbation equations (obtained in Ref. [25]) can be reduced to a single modified Regge-Wheeler equation for the axial modes and a system of two coupled equations for the polar modes. We subsequently applied the eikonal toolkit to these equations and analytically calculated the scalar-Gauss-Bonnet gravity modifications to the GR eikonal QNMs. Among other things, this analysis allowed us to identify a key conceptual issue, namely, the correct ordering of the two underlying approximations (small coupling limit and eikonal approximation); as a result, we have found QNMs that are in good agreement with previous numerical calculations (with the exception of the polar mode's imaginary part). The lessons learned from this study should be equally applicable to any other theory that deviates perturbatively from GR. Such theories are ubiquitous, for instance, in effective field theory inspired extensions to GR (see, e.g., Refs. [81–83]).

The present work can be extended in a number of ways. A simple generalization would be to repeat the calculation performed here using a higher α -order black hole background; this would globally improve the agreement between the eikonal formulas and the numerical results of Ref. [25]. A more sophisticated approach would be to abandon altogether the small-coupling approximation and work directly with a numerically determined black hole background. A nonperturbative calculation along these lines would bring closer the eikonal and numerical QNM results across the entire range of α . More importantly, this calculation may allow the eikonal study of QNMs of spontaneously scalarized Gauss-Bonnet black holes [26,27] or perhaps even shed some more light on the mechanism of spontaneous scalarization itself. It is also of interest to investigate the implications of losing hyperbolicity in Eqs. (3.17)–(3.19), for the case of spontaneous scalarization as found in Refs. [26–28] and the existence of a second branch of modes that appears for larger Gauss-Bonnet and dilaton couplings, as found in Ref. [29]. This should be studied in future work.

Another particularly important direction is to extend our calculation for rotating black hole spacetimes. A first step in this direction has been taken in Ref. [70], which worked perturbatively, to leading order in spin, on a parametrized pair of coupled wave equations. The strategy used in Ref. [70] could be applied to the already analytically known slowly rotating black hole solutions in scalar-Gauss-Bonnet gravity [84,85] for which the perturbation

equations could be obtained using the methods of Refs. [86–91] and the QNM spectra calculated in Ref. [37].

Finally, from a conceptual point of view, it would be interesting to explore whether the geometrical optics–null geodesic correspondence, which was established here for the tensorial axial perturbations (described by a single wave equation), can be generalized to systems of coupled wave equations.

ACKNOWLEDGMENTS

We thank Helvi Witek for discussions and also Caio F. B. Macedo for sharing unpublished numerical data used in this work. K. Y. acknowledges support from NSF Grant No. PHY-1806776, NASA Grant No. 80NSSC20K0523, a Sloan Foundation Research Fellowship, the Owens Family Foundation, and JSPS KAKENHI Grant

No. JP17H06358. K. Y. and K. G. would like to also acknowledge support by the COST Action GWverse Grant No. CA16104. H. O. S. acknowledges support by the NSF Grant No. PHY-1607130 and NASA Grants No. NNX16AB98G and No. 80NSSC17M0041.

APPENDIX: SUPPLEMENTAL EXPRESSIONS

In this Appendix, we show the explicit form of some of the functions introduced in the perturbations equations in the main text. All the expressions presented here, together with the axial perturbation potential \tilde{V}_{ax} in Eq. (3.10) and the GR polar (Zerilli) potential V_Z in Eq. (3.21), are given in the supplemental *Mathematica* notebook [77].

First, the function c in Eq. (3.4) for axial perturbations is given by

$$c = k_1 \frac{\sqrt{B}}{r} \frac{A - 2\alpha B A' \phi' f'(\phi)}{\sqrt{-2\alpha A B' \phi' f'(\phi) - 4\alpha B [\phi'^2 f''(\phi) + \phi'' f'(\phi)] + 1}}, \quad (\text{A1})$$

with some arbitrary constant k_1 .

Next, we present the functions appearing in the coupled gravitoscalar perturbation equations. The functions p_{pol} , A_{pol} , a_0 , and a_1 in the gravitational perturbation equation (3.18) are given by

$$p_{\text{pol}} = 32\alpha^2 f_0'^2 \frac{(r-2)^3 [96 + 3(8\Lambda - 1)r + \Lambda r^2 + \Lambda r^3]}{r^{10}(3 + \Lambda r)^2}, \quad (\text{A2})$$

$$A_{\text{pol}} = 1 - 16\alpha^2 f_0'^2 \frac{(r-2)[32 - 24r + 24r^2 + (8\Lambda + 11)r^3 + 3(\Lambda + 1)r^4 + \Lambda r^5]}{r^8(3 + \Lambda r)}, \quad (\text{A3})$$

$$a_0 = \frac{2\alpha f_0'}{r^8(3 + \Lambda r)^2} \{16r^4 \omega^2 (1-r)(3 + \Lambda r) + (2-r)[96 + 128\Lambda r + 8[4(\Lambda - 3)\Lambda - 21]r^2 - 16(2\Lambda^2 + \Lambda - 6)r^3 + 24\Lambda(\Lambda + 2)r^4 + 3r^5 + 2\Lambda r^6]\}, \quad (\text{A4})$$

$$a_1 = -16\alpha f_0' \frac{(r-2)[15 + (7\Lambda - 6)r - 3\Lambda r^2]}{r^5(3 + \Lambda r)^2}, \quad (\text{A5})$$

where $\Lambda = (\ell + 2)(\ell - 1)/2$. The functions in the scalar perturbation equation (3.19) are given by

$$\begin{aligned} b_0 = \alpha \Bigg\{ & -\frac{4\omega^2 f_0'(r-2)(4+r)}{r^4} + \frac{1}{r^8(3 + \Lambda r)^2} 4f_0'(r-2)[576 + 18(8\Lambda - 17)r \\ & - 3[22\Lambda(2\Lambda + 3) - 3]r^2 + \Lambda[9 - 2\Lambda(40\Lambda + 37)]r^3 + \Lambda^2[5 - 2\Lambda(6\Lambda + 5)]r^4 + \Lambda^2(\Lambda + 1)r^5] \Bigg\} \\ & - \alpha^2 f_0' f_0''(r-2) \Bigg\{ \frac{\omega^2}{15r^7} (800 + 896r + 876r^2 + 292r^3 + 73r^4) \\ & - \frac{1}{15r^{11}(3 + \Lambda r)^2} [89280 + 288(70\Lambda + 59)r - 24(920\Lambda^2 + 732\Lambda - 1299)r^2 \\ & - 4[2\Lambda(8\Lambda(205\Lambda + 454) + 963) + 9063]r^3 - 2[2\Lambda(2\Lambda(4\Lambda(60\Lambda + 361) + 3145) + 5823) - 657]r^4 \\ & + [657 - 2\Lambda(720\Lambda^3 + 5468\Lambda^2 + 4310\Lambda - 657)]r^5 + \Lambda[657 - 2\Lambda(720\Lambda^2 + 574\Lambda - 365)]r^6 \\ & + 73\Lambda^2(2\Lambda + 5)r^7 + 73\Lambda^2(\Lambda + 1)r^8] \Bigg\}, \quad (\text{A6}) \end{aligned}$$

$$b_1 = \frac{4\alpha f'_0(r-2)[96+3(8\Lambda-1)r+\Lambda r^2+\Lambda r^3]}{r^6(3+\Lambda r)} + \frac{\alpha^2 f'_0 f''_0}{15r^9(3+\Lambda r)}(r-2)[14880+96(35\Lambda+107)r+4(608\Lambda+2583)r^2+4(647\Lambda-219)r^3-219r^4+73\Lambda r^5+73\Lambda r^6]. \quad (\text{A7})$$

The scalar potential in Eq. (3.19) is only needed to $\mathcal{O}(\alpha)$ since $\phi_1(r)$ is already $\mathcal{O}(\alpha)$:

$$V_\phi = \frac{2}{r^4}(r-2)(1+\Lambda r+r) - \alpha f''_0 \frac{48(r-2)}{r^7}. \quad (\text{A8})$$

Finally, the scalar-Gauss-Bonnet correction to the potential for gravitational perturbation V_2 in Eq. (3.20) is given by

$$V_2 = -\frac{(r-2)}{120r^{12}(3+\Lambda r)^3} \{8847360 + 276480(8\Lambda-49)r - 23040[4\Lambda(22\Lambda+57) - 339]r^2 - 192[10\Lambda(16\Lambda(40\Lambda-29) - 3999) + 10953]r^3 - 96[4\Lambda(5\Lambda(16\Lambda(6\Lambda-35) - 1619) + 10131) + 2241]r^4 + 24[2\Lambda(40\Lambda(\Lambda(96\Lambda-1) - 1327) - 4641) + 7353]r^5 - 4[4\Lambda(\Lambda(8\Lambda(1135\Lambda+4003) + 4299) - 9486) - 8019]r^6 + 2[4\Lambda(2\Lambda(\Lambda(68\Lambda+485) + 3744) + 12501) + 7209]r^7 + [8\Lambda(\Lambda(22\Lambda(17\Lambda+158) + 10839) + 2403) - 3969]r^8 + \Lambda[8\Lambda(\Lambda(977\Lambda+3143) + 1332) - 3969]r^9 + 9\Lambda^2[4\Lambda(23\Lambda+72) - 49]r^{10} + 147\Lambda^2[\Lambda(2\Lambda+5) + 6]r^{11}\}. \quad (\text{A9})$$

-
- [1] B. P. Abbott *et al.* (LIGO Scientific and Virgo Collaborations), Properties of the Binary Black Hole Merger GW150914, *Phys. Rev. Lett.* **116**, 241102 (2016).
- [2] B. Abbott *et al.*, GW170817: Observation of Gravitational Waves from a Binary Neutron Star Inspiral, *Phys. Rev. Lett.* **119**, 161101 (2017).
- [3] B. P. Abbott *et al.* (LIGO Scientific, Virgo and Fermi-GBM, INTEGRAL Collaborations), Gravitational waves and gamma-rays from a binary neutron star merger: GW170817 and GRB 170817A, *Astrophys. J.* **848**, L13 (2017).
- [4] B. P. Abbott *et al.* (LIGO Scientific and Virgo Collaborations), GWTC-1: A Gravitational-Wave Transient Catalog of Compact Binary Mergers Observed by LIGO and Virgo during the First and Second Observing Runs, *Phys. Rev. X* **9**, 031040 (2019).
- [5] R. Abbott *et al.* (LIGO Scientific and Virgo Collaborations), GWTC-2: Compact Binary Coalescences Observed by LIGO and Virgo During the First Half of the Third Observing Run, *Phys. Rev. X* **11**, 021053 (2021).
- [6] E. Berti *et al.*, Testing general relativity with present and future astrophysical observations, *Classical Quant. Grav.* **32**, 243001 (2015).
- [7] N. Yunes, K. Yagi, and F. Pretorius, Theoretical physics implications of the binary black-hole mergers GW150914 and GW151226, *Phys. Rev. D* **94**, 084002 (2016).
- [8] B. P. Abbott *et al.* (LIGO Scientific and Virgo Collaborations), Tests of General Relativity with GW150914, *Phys. Rev. Lett.* **116**, 221101 (2016); Erratum, *Phys. Rev. Lett.* **121**, 129902 (2018).
- [9] B. P. Abbott *et al.* (LIGO Scientific and Virgo Collaborations), Tests of general relativity with the binary black hole signals from the LIGO-Virgo catalog GWTC-1, *Phys. Rev. D* **100**, 104036 (2019).
- [10] B. P. Abbott *et al.* (LIGO Scientific and Virgo Collaborations), Tests of General Relativity with GW170817, *Phys. Rev. Lett.* **123**, 011102 (2019).
- [11] E. Berti, K. Yagi, and N. Yunes, Extreme gravity tests with gravitational waves from compact binary coalescences: (I) Inspiral-merger, *Gen. Relativ. Gravit.* **50**, 46 (2018).
- [12] R. Nair, S. Perkins, H. O. Silva, and N. Yunes, Fundamental Physics Implications for Higher-Curvature Theories from Binary Black Hole Signals in the LIGO-Virgo Catalog GWTC-1, *Phys. Rev. Lett.* **123**, 191101 (2019).
- [13] S. E. Perkins, R. Nair, H. O. Silva, and N. Yunes, Improved gravitational-wave constraints on higher-order curvature theories of gravity, *arXiv:2104.11189*.
- [14] A. Ghosh *et al.*, Testing general relativity using golden black-hole binaries, *Phys. Rev. D* **94**, 021101 (2016).
- [15] A. Ghosh, N. K. Johnson-Mcdaniel, A. Ghosh, C. K. Mishra, P. Ajith, W. Del Pozzo, C. P. L. Berry, A. B. Nielsen, and L. London, Testing general relativity using gravitational wave signals from the inspiral, merger and ringdown of binary black holes, *Classical Quant. Grav.* **35**, 014002 (2018).

- [16] Z. Carson and K. Yagi, Probing string-inspired gravity with the inspiral–merger–ringdown consistency tests of gravitational waves, *Classical Quant. Grav.* **37**, 215007 (2020).
- [17] Z. Carson and K. Yagi, Probing beyond-Kerr spacetimes with inspiral-ringdown corrections to gravitational waves, *Phys. Rev. D* **101**, 084050 (2020).
- [18] E. Berti, K. Yagi, H. Yang, and N. Yunes, Extreme gravity tests with gravitational waves from compact binary coalescences: (II) Ringdown, *Gen. Relativ. Gravit.* **50**, 49 (2018).
- [19] M. Isi, M. Giesler, W. M. Farr, M. A. Scheel, and S. A. Teukolsky, Testing the No-Hair Theorem with GW150914, *Phys. Rev. Lett.* **123**, 111102 (2019).
- [20] E. Berti, V. Cardoso, and C. M. Will, On gravitational-wave spectroscopy of massive black holes with the space interferometer LISA, *Phys. Rev. D* **73**, 064030 (2006).
- [21] C. D. Capano, M. Cabero, J. Abedi, S. Kasta, J. Westerbeek, A. H. Nitz, A. B. Nielsen, and B. Krishnan, Observation of a multimode quasi-normal spectrum from a perturbed black hole, [arXiv:2105.05238](https://arxiv.org/abs/2105.05238).
- [22] N. Yunes and C. F. Sopuerta, Perturbations of Schwarzschild black holes in Chern-Simons modified gravity, *Phys. Rev. D* **77**, 064007 (2008).
- [23] V. Ferrari, M. Pauri, and F. Piazza, Quasinormal modes of charged, dilaton black holes, *Phys. Rev. D* **63**, 064009 (2001).
- [24] C. Molina, P. Pani, V. Cardoso, and L. Gualtieri, Gravitational signature of Schwarzschild black holes in dynamical Chern-Simons gravity, *Phys. Rev. D* **81**, 124021 (2010).
- [25] J. L. Blázquez-Salcedo, C. F. B. Macedo, V. Cardoso, V. Ferrari, L. Gualtieri, F. S. Khoo, J. Kunz, and P. Pani, Perturbed black holes in Einstein-dilaton-Gauss-Bonnet gravity: Stability, ringdown, and gravitational-wave emission, *Phys. Rev. D* **94**, 104024 (2016).
- [26] J. L. Blázquez-Salcedo, D. D. Doneva, S. Kahlen, J. Kunz, P. Nedkova, and S. S. Yazadjiev, Polar quasinormal modes of the scalarized Einstein-Gauss-Bonnet black holes, *Phys. Rev. D* **102**, 024086 (2020).
- [27] J. L. Blázquez-Salcedo, D. D. Doneva, S. Kahlen, J. Kunz, P. Nedkova, and S. S. Yazadjiev, Axial perturbations of the scalarized Einstein-Gauss-Bonnet black holes, *Phys. Rev. D* **101**, 104006 (2020).
- [28] J. L. Blázquez-Salcedo, D. D. Doneva, J. Kunz, and S. S. Yazadjiev, Radial perturbations of the scalarized Einstein-Gauss-Bonnet black holes, *Phys. Rev. D* **98**, 084011 (2018).
- [29] J. L. Blázquez-Salcedo, F. S. Khoo, and J. Kunz, Quasinormal modes of Einstein-Gauss-Bonnet-dilaton black holes, *Phys. Rev. D* **96**, 064008 (2017).
- [30] R. Brito and C. Pacilio, Quasinormal modes of weakly charged Einstein-Maxwell-dilaton black holes, *Phys. Rev. D* **98**, 104042 (2018).
- [31] J. Bao, C. Shi, H. Wang, J.-D. Zhang, Y. Hu, J. Mei, and J. Luo, Constraining modified gravity with ringdown signals: An explicit example, *Phys. Rev. D* **100**, 084024 (2019).
- [32] F. Moulin, A. Barrau, and K. Martineau, An overview of quasinormal modes in modified and extended gravity, *Universe* **5**, 202 (2019).
- [33] O. J. Tattersall and P. G. Ferreira, Quasinormal modes of black holes in Horndeski gravity, *Phys. Rev. D* **97**, 104047 (2018).
- [34] O. J. Tattersall and P. G. Ferreira, Forecasts for low spin black hole spectroscopy in Horndeski gravity, *Phys. Rev. D* **99**, 104082 (2019).
- [35] P. A. Cano, K. Fransen, and T. Hertog, Ringing of rotating black holes in higher-derivative gravity, *Phys. Rev. D* **102**, 044047 (2020).
- [36] P. K. Wagle, N. Yunes, and H. O. Silva, Quasinormal modes of slowly-rotating black holes in dynamical Chern-Simons gravity, [arXiv:2103.09913](https://arxiv.org/abs/2103.09913).
- [37] L. Pierini and L. Gualtieri, Quasi-normal modes of rotating black holes in Einstein-dilaton Gauss-Bonnet gravity: The first order in rotation, *Phys. Rev. D* **103**, 124017 (2021).
- [38] K. Glampedakis, G. Pappas, H. O. Silva, and E. Berti, Post-Kerr black hole spectroscopy, *Phys. Rev. D* **96**, 064054 (2017).
- [39] R. Brito, A. Buonanno, and V. Raymond, Black-hole spectroscopy by making full use of gravitational-wave modeling, *Phys. Rev. D* **98**, 084038 (2018).
- [40] V. Cardoso, M. Kimura, A. Maselli, E. Berti, C. F. B. Macedo, and R. McManus, Parametrized black hole quasinormal ringdown: Decoupled equations for nonrotating black holes, *Phys. Rev. D* **99**, 104077 (2019).
- [41] R. McManus, E. Berti, C. F. B. Macedo, M. Kimura, A. Maselli, and V. Cardoso, Parametrized black hole quasinormal ringdown. II. Coupled equations and quadratic corrections for nonrotating black holes, *Phys. Rev. D* **100**, 044061 (2019).
- [42] A. Maselli, P. Pani, L. Gualtieri, and E. Berti, Parametrized ringdown spin expansion coefficients: A data-analysis framework for black-hole spectroscopy with multiple events, *Phys. Rev. D* **101**, 024043 (2020).
- [43] M. Kimura, Note on the parametrized black hole quasinormal ringdown formalism, *Phys. Rev. D* **101**, 064031 (2020).
- [44] R. Abbott *et al.* (LIGO Scientific and Virgo Collaborations), Tests of general relativity with binary black holes from the second LIGO-Virgo gravitational-wave transient catalog, *Phys. Rev. D* **103**, 122002 (2021).
- [45] G. Carullo, Enhancing modified gravity detection from gravitational-wave observations using the parametrized ringdown spin expansion coefficients formalism, *Phys. Rev. D* **103**, 124043 (2021).
- [46] A. Ghosh, R. Brito, and A. Buonanno, Constraints on quasinormal-mode frequencies with LIGO-Virgo binary-black-hole observations, *Phys. Rev. D* **103**, 124041 (2021).
- [47] G. Antoniou, A. Bakopoulos, and P. Kanti, Evasion of No-Hair Theorems and Novel Black-Hole Solutions in Gauss-Bonnet Theories, *Phys. Rev. Lett.* **120**, 131102 (2018).
- [48] G. Antoniou, A. Bakopoulos, and P. Kanti, Black-hole solutions with scalar hair in Einstein-scalar-Gauss-Bonnet theories, *Phys. Rev. D* **97**, 084037 (2018).
- [49] D. J. Gross and J. H. Sloan, The quartic effective action for the heterotic string, *Nucl. Phys.* **B291**, 41 (1987).
- [50] R. R. Metsaev and A. A. Tseytlin, Order α' (two loop) equivalence of the string equations of motion and the sigma model Weyl invariance conditions: Dependence on the dilaton and the antisymmetric tensor, *Nucl. Phys.* **B293**, 385 (1987).

- [51] P. Kanti, N. E. Mavromatos, J. Rizos, K. Tamvakis, and E. Winstanley, Dilatonic black holes in higher curvature string gravity, *Phys. Rev. D* **54**, 5049 (1996).
- [52] K.-I. Maeda, N. Ohta, and Y. Sasagawa, Black hole solutions in string theory with Gauss-Bonnet curvature correction, *Phys. Rev. D* **80**, 104032 (2009).
- [53] N. Yunes and L. C. Stein, Non-spinning black holes in alternative theories of gravity, *Phys. Rev. D* **83**, 104002 (2011).
- [54] K. Yagi, L. C. Stein, N. Yunes, and T. Tanaka, Post-Newtonian, quasi-circular binary inspirals in quadratic modified gravity, *Phys. Rev. D* **85**, 064022 (2012); Erratum, *Phys. Rev. D* **93**, 029902 (2016).
- [55] T. P. Sotiriou and S.-Y. Zhou, Black Hole Hair in Generalized Scalar-Tensor Gravity, *Phys. Rev. Lett.* **112**, 251102 (2014).
- [56] T. P. Sotiriou and S.-Y. Zhou, Black hole hair in generalized scalar-tensor gravity: An explicit example, *Phys. Rev. D* **90**, 124063 (2014).
- [57] K. Yagi, L. C. Stein, and N. Yunes, Challenging the presence of scalar charge and dipolar radiation in binary pulsars, *Phys. Rev. D* **93**, 024010 (2016).
- [58] H. O. Silva, J. Sakstein, L. Gualtieri, T. P. Sotiriou, and E. Berti, Spontaneous Scalarization of Black Holes and Compact Stars from a Gauss-Bonnet Coupling, *Phys. Rev. Lett.* **120**, 131104 (2018).
- [59] A. Dima, E. Barausse, N. Franchini, and T. P. Sotiriou, Spin-Induced Black Hole Spontaneous Scalarization, *Phys. Rev. Lett.* **125**, 231101 (2020).
- [60] E. Berti, L. G. Collodel, B. Kleihaus, and J. Kunz, Spin-Induced Black-Hole Scalarization in Einstein-Scalar-Gauss-Bonnet Theory, *Phys. Rev. Lett.* **126**, 011104 (2021).
- [61] H. O. Silva, H. Witek, M. Elley, and N. Yunes, Dynamical scalarization and descalarization in binary black hole mergers, *arXiv:2012.10436*.
- [62] D. D. Doneva and S. S. Yazadjiev, New Gauss-Bonnet Black Holes with Curvature-Induced Scalarization in Extended Scalar-Tensor Theories, *Phys. Rev. Lett.* **120**, 131103 (2018).
- [63] D. D. Doneva and S. S. Yazadjiev, Neutron star solutions with curvature induced scalarization in the extended Gauss-Bonnet scalar-tensor theories, *J. Cosmol. Astropart. Phys.* **04** (2018) 011.
- [64] H. O. Silva, C. F. B. Macedo, T. P. Sotiriou, L. Gualtieri, J. Sakstein, and E. Berti, Stability of scalarized black hole solutions in scalar-Gauss-Bonnet gravity, *Phys. Rev. D* **99**, 064011 (2019).
- [65] M. Minamitsuji and T. Ikeda, Scalarized black holes in the presence of the coupling to Gauss-Bonnet gravity, *Phys. Rev. D* **99**, 044017 (2019).
- [66] C. F. B. Macedo, J. Sakstein, E. Berti, L. Gualtieri, H. O. Silva, and T. P. Sotiriou, Self-interactions and spontaneous black hole scalarization, *Phys. Rev. D* **99**, 104041 (2019).
- [67] N. Andreou, N. Franchini, G. Ventagli, and T. P. Sotiriou, Spontaneous scalarization in generalised scalar-tensor theory, *Phys. Rev. D* **99**, 124022 (2019); Erratum, *Phys. Rev. D* **101**, 109903 (2020).
- [68] C. A. R. Herdeiro, E. Radu, H. O. Silva, T. P. Sotiriou, and N. Yunes, Spin-Induced Scalarized Black Holes, *Phys. Rev. Lett.* **126**, 011103 (2021).
- [69] K. Glampedakis and H. O. Silva, Eikonal quasinormal modes of black holes beyond general relativity, *Phys. Rev. D* **100**, 044040 (2019).
- [70] H. O. Silva and K. Glampedakis, Eikonal quasinormal modes of black holes beyond general relativity. II. Generalized scalar-tensor perturbations, *Phys. Rev. D* **101**, 044051 (2020).
- [71] S. Mignemi and N. Stewart, Charged black holes in effective string theory, *Phys. Rev. D* **47**, 5259 (1993).
- [72] J. F. Delgado, C. A. Herdeiro, and E. Radu, Spinning black holes in shift-symmetric Horndeski theory, *J. High Energy Phys.* **04** (2020) 180.
- [73] S. Alexeev and M. Pomazanov, Black hole solutions with dilatonic hair in higher curvature gravity, *Phys. Rev. D* **55**, 2110 (1997).
- [74] F.-L. Julié and E. Berti, Post-Newtonian dynamics and black hole thermodynamics in Einstein-scalar-Gauss-Bonnet gravity, *Phys. Rev. D* **100**, 104061 (2019).
- [75] T. Regge and J. A. Wheeler, Stability of a Schwarzschild singularity, *Phys. Rev.* **108**, 1063 (1957).
- [76] F. J. Zerilli, Effective Potential for Even Parity Regge-Wheeler Gravitational Perturbation Equations, *Phys. Rev. Lett.* **24**, 737 (1970).
- [77] https://github.com/KentYagi/sGB_eikonal.git.
- [78] V. Ferrari and B. Mashhoon, New approach to the quasinormal modes of a black hole, *Phys. Rev. D* **30**, 295 (1984).
- [79] V. Cardoso, A. S. Miranda, E. Berti, H. Witek, and V. T. Zanchin, Geodesic stability, Lyapunov exponents and quasinormal modes, *Phys. Rev. D* **79**, 064016 (2009).
- [80] H. Yang, D. A. Nichols, F. Zhang, A. Zimmerman, Z. Zhang, and Y. Chen, Quasinormal-mode spectrum of Kerr black holes and its geometric interpretation, *Phys. Rev. D* **86**, 104006 (2012).
- [81] S. Endlich, V. Gorbenko, J. Huang, and L. Senatore, An effective formalism for testing extensions to general relativity with gravitational waves, *J. High Energy Phys.* **09** (2017) 122.
- [82] V. Cardoso, M. Kimura, A. Maselli, and L. Senatore, Black Holes in an Effective Field Theory Extension of General Relativity, *Phys. Rev. Lett.* **121**, 251105 (2018).
- [83] P. A. Cano and A. Ruipérez, Leading higher-derivative corrections to Kerr geometry, *J. High Energy Phys.* **05** (2019) 189; Erratum, *J. High Energy Phys.* **03** (2020) 187.
- [84] P. Pani, C. F. Macedo, L. C. Crispino, and V. Cardoso, Slowly rotating black holes in alternative theories of gravity, *Phys. Rev. D* **84**, 087501 (2011).
- [85] A. Maselli, P. Pani, L. Gualtieri, and V. Ferrari, Rotating black holes in Einstein-Dilaton-Gauss-Bonnet gravity with finite coupling, *Phys. Rev. D* **92**, 083014 (2015).
- [86] Y. Kojima, Equations governing the nonradial oscillations of a slowly rotating relativistic star, *Phys. Rev. D* **46**, 4289 (1992).
- [87] Y. Kojima, Normal modes of relativistic stars in slow rotation limit, *Astrophys. J.* **414**, 247 (1993).
- [88] Y. Kojima, Coupled pulsations between polar and axial modes in a slowly rotating relativistic star, *Prog. Theor. Phys.* **90**, 977 (1993).

-
- [89] P. Pani, V. Cardoso, L. Gualtieri, E. Berti, and A. Ishibashi, Black Hole Bombs and Photon Mass Bounds, *Phys. Rev. Lett.* **109**, 131102 (2012).
- [90] P. Pani, V. Cardoso, L. Gualtieri, E. Berti, and A. Ishibashi, Perturbations of slowly rotating black holes: Massive vector fields in the Kerr metric, *Phys. Rev. D* **86**, 104017 (2012).
- [91] P. Pani, Advanced methods in black-hole perturbation theory, *Int. J. Mod. Phys. A* **28**, 1340018 (2013).